INVITED PAPERS

Improved carbon dioxide gas sensing features of zinc oxide nanorods assisted by an organic filler for dynamic situations

Mohammad Mehdi Shokravi[1] · Shahruz Nasirian[1]

Abstract

Zinc oxide (ZnO) nanorods prepared by a simple hydrothermal method. The characterization of the sample revealed the formation of the ZnO nanorods with hexagonal wurtzite structure. The CO_2 sensing properties of the resistive-type sensor based on ZnO nanorods assisted by polyvinyl alcohol (ZFS) investigated as a function of gas concentration and relative humidity (RH) at room temperature. The response and response time of the ZFS reduced with increasing RH from 30 to 90% at various gas levels. The sensor showed the highest response of 120.3% at 0.3 vol% CO_2 and 30% RH, while it exhibited a proper response of 81% at 90% RH and 0.037 vol% CO_2. Moreover, the lowest response time (recovery time) of 51.3 s (34 s) at 0.3 (0.037) vol% CO_2 and 90% RH was obtained. We found that our hand-made sensor has superior response features at dynamic conditions, a good CO_2 selectivity, and long-term stability. Finally, the probable CO_2 sensing mechanism of the ZFS was discussed in detail.

Graphic abstract
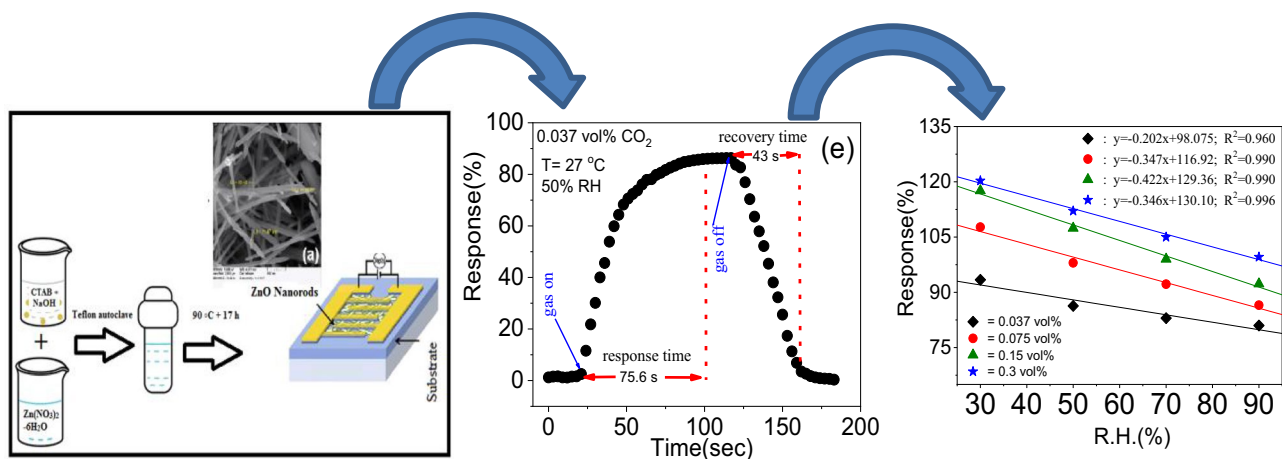
1 Introduction

In near years, the world's countries reached a joint action to limit global warming, an important idea in an international effort to keep the earth from reaching catastrophic levels.

Although the carbon dioxide gas (CO_2) is an essential component for the photosynthesis of the planets, however, it is one of the main greenhouse gases that directly contribute to global warming [1–3]. The CO_2 is a colorless, odorless and non-flammable gas that enters the atmosphere through respiration, deforestation, manufactories and burning fossil fuels [2–5]. Moreover, it is reported that the prolonged breathing of CO_2 (>5000 ppm) can cause some symptoms and respiratory disorders in humans [2–7]. Hence, the detection and monitoring of CO_2 levels at different humidity by smart

✉ Shahruz Nasirian
shahruznasirian@ustmb.ac.ir; shahruznasirian@gmail.com

1   Department of Electrical and Medical Engineering, Mazandaran University of Science and Technology, Sardaran 12 Avenue, Sheikh Tabarsi Street, P.O. Box: 734, Babol, Iran

sensors for many applications such as greenhouses, exhaust systems, air-conditioning and biotechnological processes is necessary [1, 3, 8]. The many efforts have been focused on developing several kinds of CO_2 sensors based on organic and inorganic materials such as semiconductor metal oxides (SMOs) [6–17]. Among them, the CO_2 resistive-type sensors based on n-type SMOs are widely considered to have a good reliability, accuracy, small size and low-cost production [3, 6–13]. One of the n-type SMOs with a wide band gap of 3.37 eV, a large exciton binding energy of 60 meV, non-toxicity, high electron mobility, easy to be prepared, appropriate response toward CO_2 concentrations, is zinc oxide (ZnO) [3, 6, 7, 12, 15].

Kannan et al. [3] have reported CO_2 sensor based on nanostructured ZnO thin films which had the response and the response/recovery time of 1.13% and 20/20 s, respectively, toward 1000 ppm CO_2 concentration at 300 °C operating temperature. Renn Juang et al. [6] developed the ZnO nanorods structure for a CO_2 sensor. They have measured the sensor response, response time and recovery time of about 354%, 10 s and 18 s, respectively, toward 2500 ppm CO_2 at 150 °C operating temperature. Righettoni et al. [12] reported the chemo-resistive CO_2 sensor based on ZnO nanoplatelets. Their measured sensor response was 2% toward 1000 ppm CO_2 concentration at 350 °C operating temperature.

According to the mentioned reports, the ZnO based CO_2 sensors have shown a considerable response only at the elevated operating temperatures (>150 °C) regardless of humidity levels. It is reported that the gas adsorption on a sensor surface can be enhanced by increasing the operating temperature [3, 4, 6, 7]. However, the result of high operating temperature in a resistive-type CO_2 sensor is the poor long-term stability and high power consumption.

To avoid these problems, the CO_2 detection at low operating temperature is needed. In this regard, humidity poses another great challenge [18, 19], because the increase of the humidity significantly impedes the response of the resistive-type CO_2 sensor based on the ZnO. It is described that the ambient oxygen molecules can accept electrons from the n-type ZnO at low temperature and humidity, which the result is the creation of the negatively charged oxygen species (O_2^-), formation of the depletion region on the sensor surface elements, and reduction of the ZnO surface active sites [3, 7, 18–21]. This insulated barrier on the sensor surface causes the CO_2 molecules with stable structure and covalence bonds can not react with sensor active sites. On the other hand, the active sites of the CO_2 sensor based on the ZnO fill with more O_2^- ions and water molecules at low temperature and high humidity. The result is a lower sensor response than that low humidity condition [7, 15]. Accordingly, it seems the reduction of the surface depletion region and oxygen ions, and the increase of the gas levels detection ability at different humidity are effective factors

to enhanced performance of the resistive-type CO_2 sensor based on the ZnO. The use of moisture-sensitive organic filler on the nanostructures of the ZnO is one promising strategy to improve the sensor performance [22–25]. Zhou et al. [16] reported a surface acoustic wave sensors based on silicon-based polymers with good response toward CO_2 concentrations at 70 °C operating temperature and 70% humidity. In this regard, polyvinyl alcohol (PVA) with superior film-filling properties is a great O_2 barrier and sensitive to water molecules, which it can enhance the efficiency of the CO_2 gas sensor at different humidity [22–25]. However, it still needs more study on reliable resistive-type CO_2 sensor with ability to work at different humidity.

In this paper, we present a simple one-step method to fabricate the 1D-ZnO nanostructures through the hydrothermal method. The ZnO nanostructures assisted by PVA used as CO_2 resistive-type sensor at room temperature and various relative humidity (RH).

2 Experimental

2.1 Materials and methods

Zinc nitrate hexahydrate ($Zn(NO_3)_2 \cdot 6H_2O$-99% purity), Cetyltrimethylammonium bromide (CTAB-99% purity), ethanol (99.8% purity), hydrochloric acid (HCl-36% concentrated), sodium hydroxide (98% purity), and polyvinyl alcohol (PVA) were purchased from Merck Co, and used for synthesis of the sample.

0.15 g and 2.85 g of CTAB and NaOH, respectively, were dissolved into 40 mL of distilled water to form a transparent solution under vigorous stirring (solution (A)). 4.64 g of $Zn(NO_3)_2 \cdot 6H_2O$ was dissolved into 40 mL of distilled water under vigorous stirring (solution (B)). Then, the solution (B) was slowly added to the solution (A) under continuous stirring. After 3 h vigorous stirring, the resulted solution was transferred to a Teflon autoclave of 150 mL capacity and was heated at 90 °C for 17 h. The obtained white sediment solid product was filtered and washed with distilled water and absolute ethanol several times, and was dried in oven at 100 °C. The obtained ZnO powder was used as the sensitive CO_2 material.

One gram of PVA was added into 99 mL of deionized water and the result was heated at 90 °C for 3 h under vigorous stirring to obtain a transparent PVA solution of 1 wt%. 2 g of the ZnO nanopowder was added in 10 mL of deionized water and the result was ultrasonicated for 15 min and magnetically stirred for 2 h to achieve a milky solution. The prepared solution was added into the 3 mL of 1 wt% PVA solution, and then it was stirred carefully by magnetic stirring to obtain a solution containing the ZnO nanostructures. Finger type Cu-interdigited electrodes were patterned onto

20×20 mm^2 area of an epoxy glass substrate for sensor substrate preparation. The prepared homogenous solution was deposited on the cleaned sensor substrate using the spin coating technique at a speed of 500 RPM and dried under a vacuum oven at 100 °C. The prepared sensor based on the film of the ZnO nanorods assisted by PVA was briefly called ZFS. The gas sensing experiment was carried out in an enclosed polyethylene chamber. The sensor response is defined as [3, 4, 7]:

$$\text{Response } (\%) \; = \; \left| \left(R_{\text{air}} - R_{\text{gas}} \right) / R_{\text{air}} \right| \; \times \; 100 \qquad (1)$$

where R_{air} and R_{gas} are the resistance of sensor in air and gas atmosphere, respectively. The response time and recovery time are important parameters used for characterizing a sensor [4, 6] and they are defined as the time required to reach 90% of the final change in resistance, when the gas is turned on and off, respectively.

2.2 Characterization

X-ray diffractometry (XRD) was carried out using Philips-PW 1730 X-ray diffractometer with copper radiation (Cu-Ka, $\lambda = 1.54$ Å) through a graphite monochromator and step-scanning measurements in a range from 10° to 80° 2θ, with a step of 0.04 2θ and a working voltage of 30 kV. The morphological characterization analysis was carried out by field-effect scanning electron microscopy (FESEM) using a TES-CAN- MRIA3 instrument at 15 kV, equipped with an energy dispersive X-ray spectroscopy (EDX) detector. The specific surface area was analyzed by Brunauer–Emmett–Teller spectroscopy (BET) method using a BELSORP-MR6 instrument via Nitrogen adsorption–desorption measurements.

3 Results and discussion

3.1 The ZnO characterization

The XRD pattern of the ZnO thin film (ZTF) in Fig. 1a shows all diffraction peaks have been matched well with standard diffraction pattern data of the ZnO (JCPDS card No. 98-006-5172). A series of diffraction peaks can be seen at $2\theta = 31.8, 34.5, 36.3, 47.6, 56.6, 62.9, 67.9°$ that corresponding to (100) (002) (101) (102) (110) (103) (112) of hexagonal wurtzite of the ZnO crystal structure, respectively [20, 26–28]. No other impurity phases are detected from the figure. Thus, the results clearly show that the product is pure crystalized ZnO.

Morphology plays an important role in governing the sensor-response kinetics. The typical FESEM image in Fig. 1b clearly displays morphology of nanorods/nanowires for the prepared ZTF with large surface-to-volume ratio. In spite,
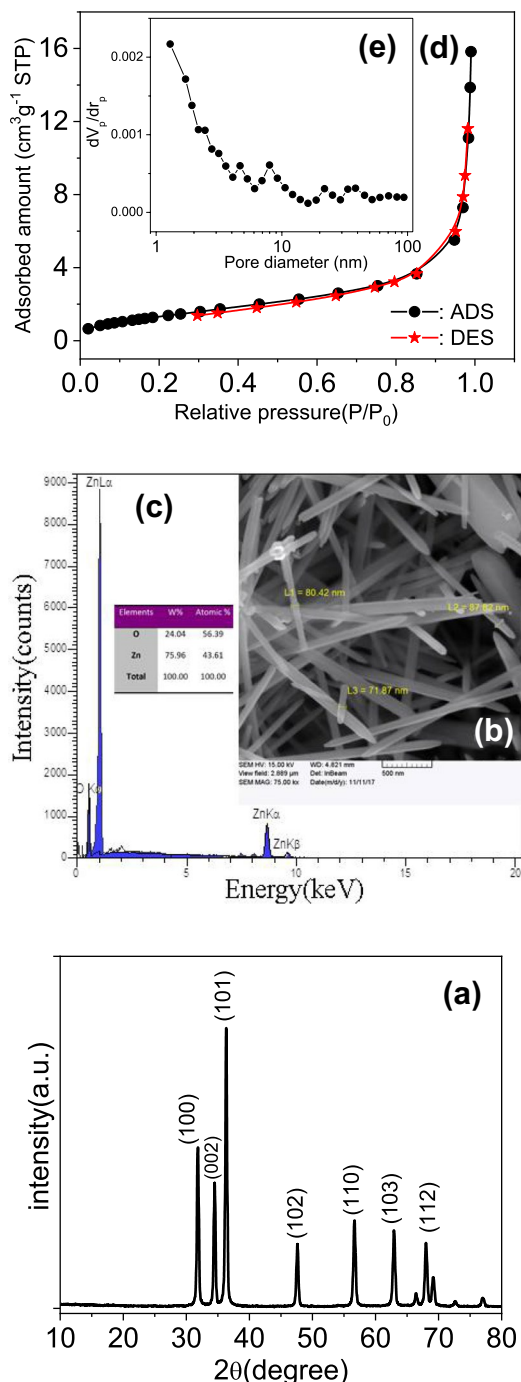
Fig. 1 a XRD pattern of the ZnO sample. **b** FESEM image and **c** EDX pattern of prepared ZnO nanorods. **d** N$_2$ absorption–desorption isotherms of the ZTF. **f** The pore-size distribution calculated by BJH method from the desorption curves

the fact that the 1D-nanorods show a dispersed distribution, the nanorods diameter and length are rather uniform. Careful examination of Fig. 1b reveals that the nanorods are in the range from 71.87 to 87.82 nm in diameter or more, and typical length is 2 μm or less. Figure 1c displays the EDX

spectra of the ZTF. The calculated atomic percentage is tabulated in the table of Fig. 1c. The peaks of Zn and O can be clearly observed in the EDX spectrum and no diffraction peaks from any other elements are detected that reveal the phase purity of the ZTF.

Nitrogen adsorption–desorption measurements were conducted to get more information about the inner architectures of the hierarchically porous structures. Figure 1d shows the nitrogen adsorption and desorption isotherms of the ZTF versus relative pressure (P/P_o) at the temperature of adsorption (P and P_o are the equilibrium and the saturation pressures of adsorbents, respectively). The isotherms exhibit hysteresis loop at P/P_o range of 0.4–0.8 that illustrate the existence of mesopores with the diameter of 5–50 nm [29, 30]. Moreover, at higher pressures the diagram slope shows increased uptake of adsorbate as pores become filled, inflection point typically occurs near completion of the first monolayer [23–25]. Then, the adsorbed nitrogen amount rises very steeply at $P/P_o > 0.8$, that suggests the existence of macropores (>50 nm in diameter) in the first monolayer of the sample surface [29–31]. The specific surface area of the ZTF was 7 m^2 g^{-1} and the average pore size was about 8 nm which was calculated using the BJH method and the desorption branch of the nitrogen isotherm (Fig. 1e).

3.2 The CO$_2$ sensing behavior of the sensor

It is well known that the response of a resistive-type SMO gas sensor at environmental conditions is highly influenced by RH. Therefore, the various CO$_2$ levels are used to perform gas-sensing tests at varying RH to examine RH. Moreover, a resistive-type gas sensor has a built-in variable resistor, which changes with different levels of the target gas. The lower or higher detection limit of a resistive-type sensor determines through its measurable resistance changes. Accordingly, the lower detection limit of our CO$_2$ sensor was 0.037 vol%, and other gas levels (as the multiples of 0.037 vol%) have been used to achieve the higher detection limit. Hence, the dynamic changes of the ZFS response to various CO$_2$ concentrations are measured under different RH and plotted in Fig. 2a–d. As shown in Fig. 2, the output response signal of the ZFS increased after gas injection and not only it reached a steady-state point in tens of seconds, but also it slightly increased with an increasing gas concentration in various RHs. These response shifts are mainly due to the change of adsorption of gas molecules on the components of the sensor surface [6]. Moreover, the sensor response did not significantly change with increasing gas level from 0.15 to 0.3 vol% at different RH, which is presumably due to the saturation of the sensor surface active sites. At the steady-state point, the pure air was introduced into the test chamber and the sensor response value was found to decrease rapidly and reached the baseline response value after the tens of seconds.

According to the results of Fig. 2, the dependence of the ZFS response to RH toward different CO$_2$ concentrations was calculated and tabulated in Table 1. The response changes of the ZFS have been decreased with an increasing RH in different gas levels. The highest response of 120.3% belongs to 0.3 vol% gas at 30% RH, while the lowest response of 81% belongs to 0.037 vol% gas at 90% RH. Herein, the highest response of sensor toward 0.3 vol% gas level at different RH is probably due to the penetration and interaction of very sufficient gas molecules with the surface components of the sensor.

The response and recovery behaviors are two important characteristics for evaluating the performance of a gas sensor. According to the results of Fig. 2, the ZFS response values versus RHs as the function of gas levels plotted in Fig. 3a. The response of the ZFS has been decreased in different gas levels through an increase of RH from 30 to 90%, but the shift of the response toward 0.037 vol% CO$_2$ was lower than other gas concentrations. Moreover, it seems that the effect of gas concentration on the ZFS response depends on RH levels because the more active surface sites of the sensor were occupied by water molecules at high RH that cause less reaction between gas molecules and surface-active sites occur. A linear relationship predicts between the ZFS responses and RH levels was observed in various gas concentrations, fitted to $y = ax + b$ with an acceptable regression analysis, as shown in Fig. 3a. The response/recovery time of the sensor was calculated from Fig. 2 and tabulated in Table 1. Accordingly, the response time and recovery time of the ZFS versus RH levels at different gas levels plotted in Fig. 3b and c, respectively. Figure 3b and c show that the recovery time decreases and the response time increases under a reduction of CO$_2$ level at various RHs. The increase of the response time and the decrease of recovery time are presumably due to a little reaction of the gas molecules with the sensor surface active sites in low gas concentration. Moreover, an increase of RH from 30 to 90% caused the response time and recovery time of the ZFS decrease, and a linear relationship with high accuracy between the response/recovery time and RH levels at different gas concentrations observed. In addition, the response time (the recovery time) has the highest (lowest) slop at the lowest gas concentration, which is probably due to the direct effect of water molecules on active sites of sensor at low gas level. The lowest response time (recovery time) of 51.3 s (34 s) at 0.3 (0.037) vol% CO$_2$ concentration and 90% RH was obtained. Moreover, despite that the sensor response decreased from 30 to 90% RH in various gas levels, its response time reduced. Then, the ZFS has a favorable response even in high RH. Figure 3d illustrates the long-term stability of the ZFS for several weeks. All measurements were conducted at 0.037 vol% CO$_2$ and two

Fig. 2 The dynamic sensing characteristics of ZFS at **a** 30%, **b** 50%, **c** 70%, **d** 90% RH atmosphere, a different gas concentration and operating temperature of 27 °C. **e** The resistant change of ZFS versus time toward 0.037 vol% CO_2 under a humidity of 50% RH
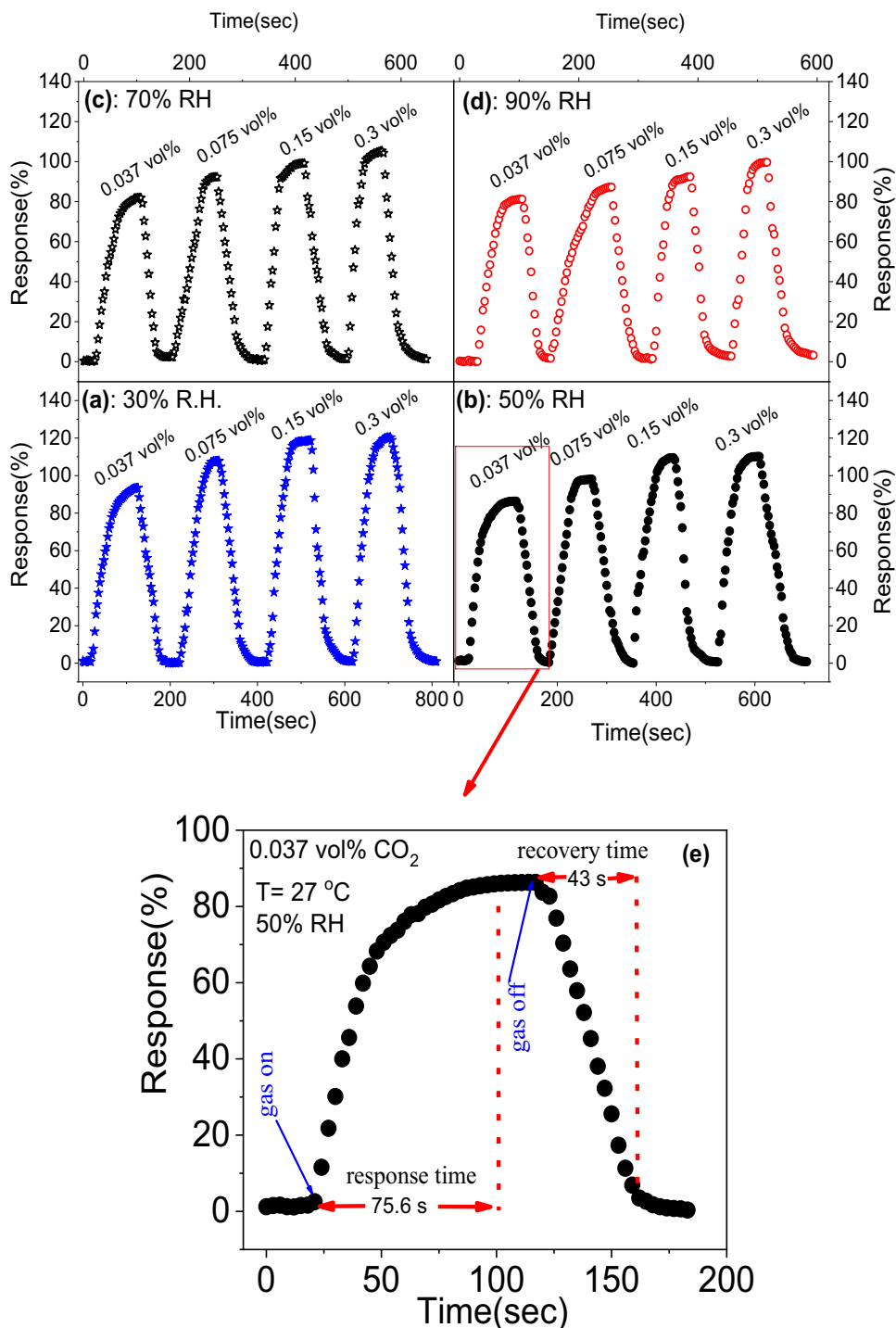
different RHs of 50% and 90%. As shown in Fig. 3d, the sensor has been demonstrated a good long-term stability with a response degradation of 9% after 14 weeks. The selectivity of the ZFS is very important because it is primarily designed to detect specific CO_2 gas under given conditions. To test the selectivity of the ZFS, it was treated with 0.037 vol% of different gases. The sensor response toward various gases at different RHs tested and plotted

in Fig. 4. This Figure shows the ZFS has good selectivity toward CO_2 at various RHs than that other gases such as O_2, N_2, H_2 and CO.

Table 2 shows a comparison between the CO_2 sensing results of the ZFS with the previous works based on the ZnO in Refs. [3, 4, 6, 7, 12]. In spite of the fact that the response/recovery time of prior reports are better than our sensor, the effect of RH on their sensing features have not

Table 1 The response, response time and recovery time of ZFS at different RH and room temperature toward various CO_2 concentrations

RH (%)	Gas concentration (vol%)	Response (%)	$t_{response}$ (s)	$t_{recovery}$ (s)
30	0.037	93.4	82.5	48.7
	0.075	107.7	79.3	75.5
	0.15	117.6	74.3	78.3
	0.3	120.3	67.5	83.7
50	0.037	86.3	75.6	43.2
	0.075	98	73	64.8
	0.15	107.4	68.8	67.5
	0.3	112.1	61	75.2
70	0.037	83	70	38
	0.075	92.2	67.1	56.7
	0.15	99	64	59.5
	0.3	105	56	67.5
90	0.037	81	63.5	34
	0.075	86.5	61	47.5
	0.15	92.3	58.5	51.3
	0.3	99.6	51.3	60.8

been investigated. Moreover, they have high operating temperature (> 150 °C), sensitivity to great gas concentration (> 1000 ppm), and low response. Moreover, our hand-made sensor has long-term stability, CO_2 gas selectivity, and a limit of detection below 0.05 vol% CO_2 at room temperature and various RHs, which offers it as a commercial reliable CO_2 sensor at dynamic conditions.

Finally, a CO_2 sensor based on the ZnO nanorods without the PVA created, and it did not show response even to 1 vol% CO_2 at room temperature and different humidity. Accordingly, the PVA is an effective organic filler to improve the efficiency of the ZnO nanorods for the CO_2 detection at room temperature and different humidity.

3.3 Gas sensing mechanism of the ZFS

Figure 5a, b shows the schematic of the possible mechanism for the ZFS response toward CO_2 levels. Because, the ZnO nanoroads covered by PVA filler, under moisture ambient, water molecules create the weakly bonds with the composite components and strong bonds with hydroxyl group in PVA units as shown in Fig. 5a [20–25]. The result of this reaction lead to the formation of the extra hydroxyl ions on the sensor surface [32–35]. In this condition, the CO_2 gas molecules react with OH⁻ part of the bound water molecules on the sensor surface and hydrolysis of the gas molecules creates bicarbonate ions, as shown in Fig. 5a [32–35]. Subsequently,

the bicarbonate ions react with not only the hydroxyl groups of the bound water molecules but also the negatively charged oxygen species. The result is secondary hydrolysis of the gas molecules and the creation of bulk carbonate ions (please see Fig. 5b). Herein, the consumption of electrons by CO_2 molecule during interaction with the sensor surface elements leads to the change of not only the sensor resistance and response but also the surface depletion layer [32, 33]. On the other hand, an increase of RH could enhance the number of the bound water molecules on the sensor surface, which leads to decrease of the surface negative charged oxygen species. According to Figs. 2 and 3 results, the decrease of the surface negative charged oxygen ions at high RH apparently caused the secondary hydrolysis of the gas molecules and the creation of the carbonate ions disrupt, which the result is the decrease of the response of the ZFS with increasing RH. As a result, the increase of RH and also the decrease of the CO_2 levels could be decreased the ZFS response at environmental conditions. The high (low) response and response time at low (high) RH and various gas levels, suggest the ZFS as a reliable device for room temperature CO_2 detection in dynamic conditions. Moreover, to check the accuracy of sensor performance, we prepared and analyzed three identical samples and they had about 3.7% deviation in the results.

4 Conclusion

In this work, 1D-nanorodes of the ZnO were synthesized by hydrothermal method and used for CO_2 detection at dynamic situations. XRD, FESEM, EDX and BET analysis confirm (a) the formation of mesoporous structure, (b) the hexagonal wurtzite structure of pure crystallized ZnO, and (c) the creation of 1D-nanorods morphology in the ZFS. The CO_2 gas sensing properties of the ZFS were carefully studied. The sensor response and selectivity were examined for low level of different gases such as CO_2, CO, N_2, O_2, H_2 and H_2O. A humidity compensation method is applied to the accuracy study of the sensor response at different RHs. The results demonstrate that the optimal sensor response depends on RH value of the test atmosphere and a linear relationship predicts between the sensor response and RH values was observed at various CO_2 concentrations. The sensor was showed the responses of 93%, 86%, 83% and 81% toward 0.037 vol% of CO_2 concentrations under 30%, 50%, 70% and 90% RH, respectively. In spite of the fact that the recovery time increased and the response time decreased with increasing CO_2 concentration at various RHs, an increase of RH from 30 to 90% led to reduce the response time and recovery time in various gas concentrations.
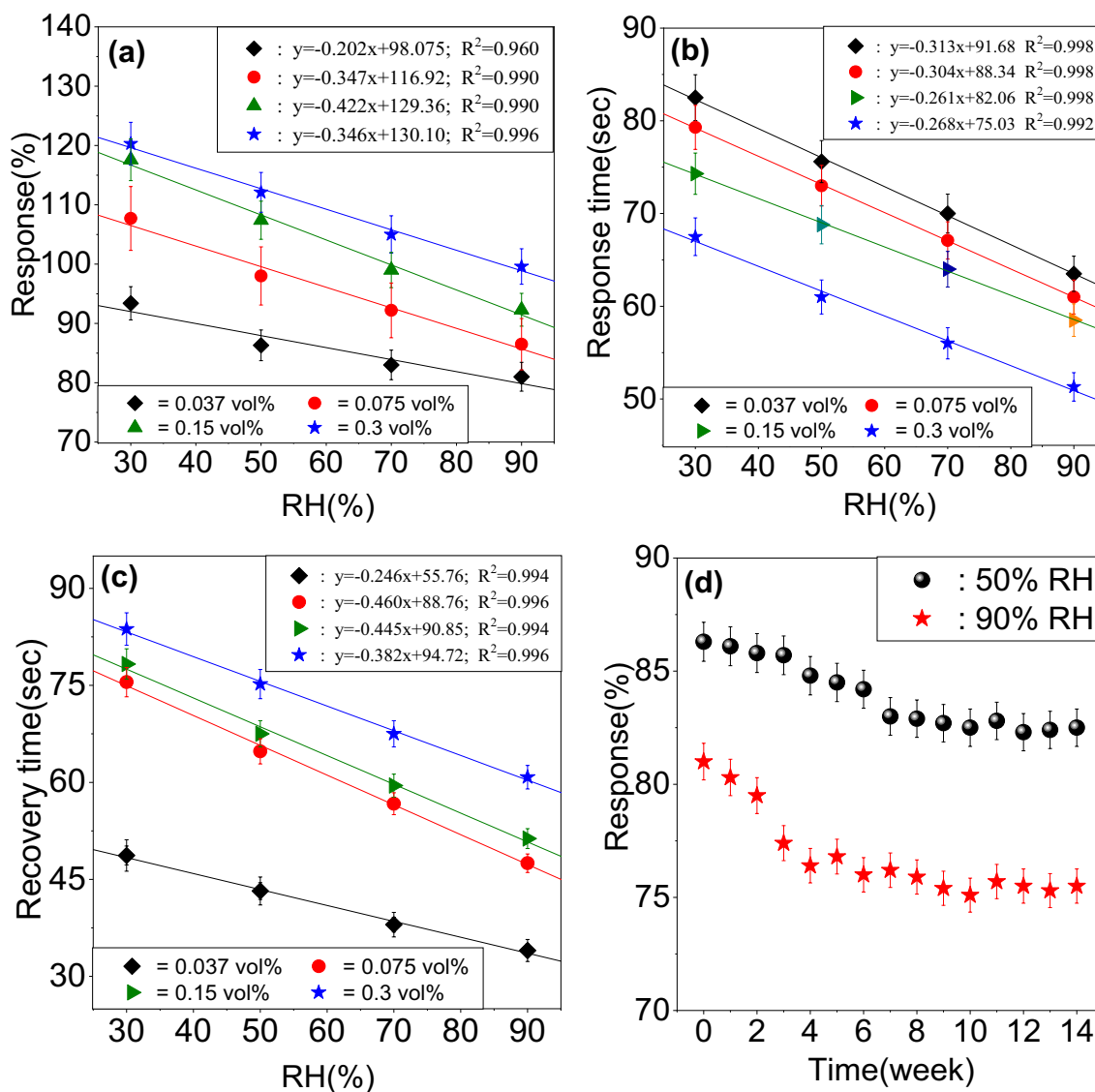
Fig. 3 **a** The response, **b** response time and **c** recovery time of ZFS versus RH with different CO_2 gas concentration at operating temperature of 27 °C. **e** The life-time stability of sensor measured during 14 weeks and end of each week. The lines are a guide for eye
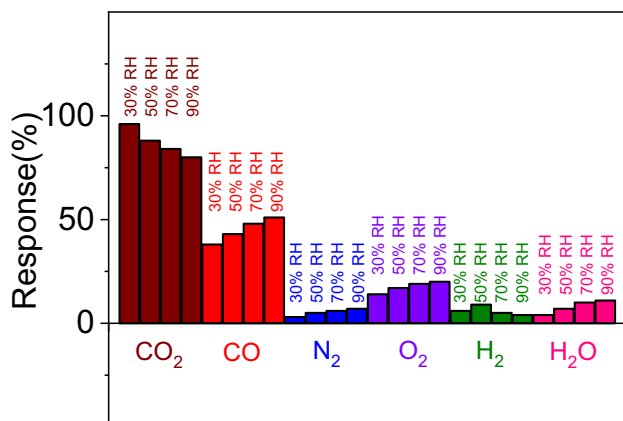
Fig. 4 The selectivity of the ZFS toward 0.037 vol% gas concentrations of CO_2, CO, N_2, O_2, H_2 and H_2O at room temperature

Table 2 Comparison of the CO_2-sensing characteristics of some sensors based on ZnO which reported in previous literatures with the prepared ZFS in the present work

Used material	Response (%)	Response time (s)	Recovery time (s)	Gas level	Operating temperature (°C)	References
ZnO	1.13	20	20	1000 ppm	300	[3]
ZnO–RGO	10	–	–	1000 ppm	200	[4]
ZnO–ZHS	354	10	18	2500 ppm	150	[6]
La loaded-ZnO	65	90	38	5000 ppm	400	[7]
ZnO	2	–	–	1000 ppm	350	[12]
ZFS at 90% RH	81	63.5	34	0.037 vol%	Room temperature	This work
ZFS at 90% RH	99.6	51.3	60.8	0.3 vol%	Room temperature	This work
ZFS at 30% RH	93.4	82.5	48.7	0.037 vol%	Room temperature	This work

Fig. 5 a The schematic diagram of the surface adsorbed oxygen and water molecules on the sensor surface and the hydrolysis of CO_2 under humidity. **b** The scheme of secondary hydrolysis of CO_2 and sensing mechanism of the ZFS
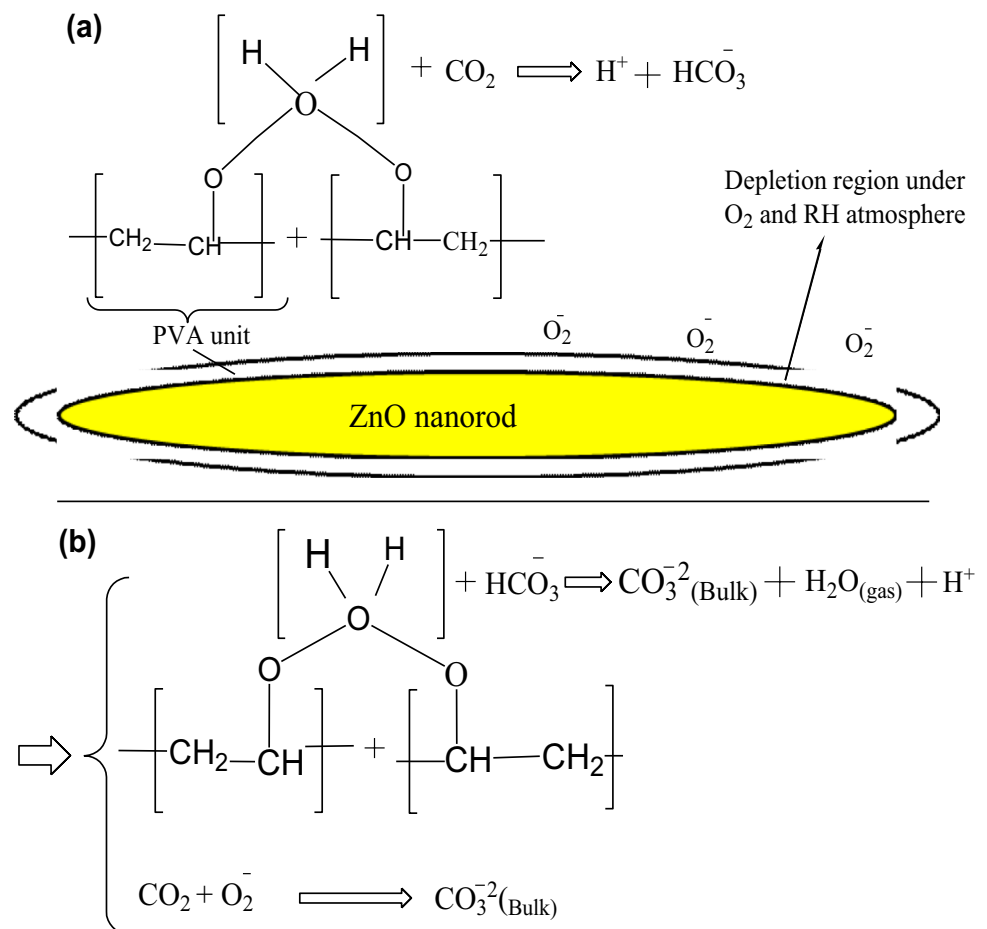
References

1. Z. Panpan, Q. Hongwei, Z. Heng, L. Wei, H. Jifan, CO_2 gas sensors based on $Yb_{1-x}Ca_xFeO_3$ nanocrystalline powders. J. Rare. Earth. **35**, 602–609 (2017)
2. M.M. Monshi, S.M. Aghaei, I. Calizo, M. M. Monshi, S. M. Aghaei, I. Calizo, Doping and defect-induced germanene: a superior media for sensing $_H2S$, S_{O2}, and C_O2 gas molecules. Surf. Sci. **665**, 96–102 (2017)
3. P. Kannan, R. Saraswathi, J.B.B. Rayappan, CO_2 gas sensing properties of DC reactive magnetron sputtered ZnO thin film. Ceram. Int. **40**, 13115–13122 (2014)
4. W.D. Hsu, J.K. Tsai, J.Y. Tang, T.H. Meen, T.C. Wu, Zinc-oxide nanorod array fabricated by high temperature hydrothermal method applied to gas sensor. Microsyst. Technol. **24**(10), 3957–3963 (2018)
5. C. Chiang, K. Tsai, Y. Lee, H. Lin, Y. Yang, C. Shih, C. Lin, H. Jeng, Y. Weng, Y. Cheng, K. Ho, C. Dai, In situ fabrication of conducting polymer composite film as a chemical resistive CO_2 gas sensor. Microelectron. Eng. **111**, 409–415 (2013)

6. F. Renn juang, W. Cherng chern, B. Yai chen, Carbon dioxide gas sensing properties of $ZnSn(OH)_6$-ZnO nanocomposites with ZnO nanorod structures. Thin Solid Films **660**, 771–776 (2018)

7. Y. Jeong, C. Balamurugan, D. Lee, Enhanced CO_2 gas-sensing performance of ZnO nanopowder by La loaded during simple hydrothermal method. Sensor. Actuat. B **229**, 288–296 (2016)

8. J. Herran, O. Gonzalez, I. Hurtado, T. Romero, G. Mandayo, E. Castano, Photoactivated solid- state gas sensor for carbon dioxide detection at room temperature. Sensor. Actuat. B **149**, 368–372 (2010)

9. M.I. Baraton, FT-IR surface study of nanosized ceramic materials used as gas sensors. Sensor. Actuat. B **31**(1–2), 33–38 (1996)

10. M.S. Nieuwenhuizen, A.J. Nederlof, A SAW gas sensor for carbon dioxide and water Preliminary experiments. Sensor. Actuat. B. **2**(2), 97–101 (1990)

11. D. Wang, Y. Chen, Z. Liu, L. Li, C. Shi, H. Qin, J. Hu, CO_2-sensing properties and mechanism of nano-SnO_2 thick- film. Sensor. Actuat. B **227**, 73–84 (2016)

12. M. Righettoni, A. Amann, S. Pratsinis, Breath analysis by nano-structured metal oxides as chemo-resistive gas sensors. Mater. Today **18**, 163–171 (2015)

13. D. Mardare, N. Comei, C. Mita, D. Florea, A. Stancu, V. Tiron, A. Manole, C. Adomnitei, Low temperature TiO_2 based gas sensors for CO_2. Ceram. Int. **42**, 7353–7359 (2016)

14. S. Naama, T. Hadjersi, A. Keffous, G. Nezzal, CO_2 gas sensor based on silicon nanowires modified with metal nanoparticles. Mat. Sci. Semicon. Proc. **38**, 367–372 (2015)

15. H. Hassan, A. Kashyout, I. Morsi, A. Nasser, I. Ali, Synthesis, characterization and fabrication of gas sensor devices using ZnO and ZnO: in nanomaterials, Beni-suef univ. J. Appl. Sci. **3**, 216–221 (2014)

16. R. Zhou, S. Vaihinger, K.E. Geckeler, W. Gopel, Reliable CO_2 sensors with silicon-based polymers on quartz microbalance transducers. Sensor. Actuat. A **18–19**, 415–420 (1994)

17. T. Lang, H.D. Wiemhofer, W. Gopel, Carbonate based CO_2 sensors with high performance. Sensor. Actuat. B **34**, 383–387 (1996)

18. V. Perekrestov, V. Latyshev, A. Kornyushchenko, Y. Kosminska, Charge transfer, structural and morphological characteristics of ZnO fractal-percolation nanosystems. J. Electron. Mater. **48**(5), 2788–2793 (2019)

19. P. Shankar, J. Rayappan, Gas sensing mechanism of metal oxides: the role of ambient atmosphere, type of semiconductor and gases. Sci. Lett. J. **4**(126), 1–18 (2015)

20. A. Jonatti, C. Van de Walle, Fundamentals of zinc oxide as a semiconductor. Rep. Prog. Phys. **72**, 1–28 (2009)

21. Q. Qi, T. Zhang, Q. Yu, R. Wang, Y. Zeng, L. Liu, H. Yang, Properties of humidity sensing ZnO nanorods-base sensor fabricated by screen-printing. Sensor. Actuat. B **133**, 638–643 (2008)

22. S.F. Hashemi Karouei, H. Milani Moghaddam, P-p heterojunction of polymer/hierarchical mesoporous $LaFeO_3$ microsphere as CO_2 gas sensing under high humidity. Appl. Surf. Sci. **479**, 1029–1038 (2019)

23. K. Ogura, H. Shiigi, A CO_2 composite film consisting of base-type polyaniline and poly (vinyl alcohol). Electrochem. Solid-State Lett. **2**, 478–480 (1999)

24. T. Oho, T. Tonosaki, K. Isomura, K. Ogura, A CO_2 sensor operating under high humidity. J. Electroanal. Chem. **522**, 173–178 (2002)

25. J.H. Jang, J.I. Han, Cylindrical relative humidity sensor based on poly-vinyl alcohol (PVA) for wearable computing devices with enhanced sensitivity. Sensor. Actuat. A. **261**, 268–273 (2017)

26. A. Nimbalkar, M. Patil, Synthesis of ZnO thin film by sol-gel spin coating technique for H_2S gas sensing application. Phys B **527**, 7–15 (2017)

27. Z. Chen, Y. Hong, Z. Lin, L. Liu, X. Zhang, Enhanced Formaldehyde Gas Sensing Properties of ZnO Nanosheets Modified with Graphene. Electron. Mater. Lett. **13**(3), 270–276 (2017)

28. H. Cakmak, S. Kahraman, F. Bayansal, S. Cetinkaya, A novel study on ZnO nanostructures: coumarin effect. Phil. Mag. Lett. **92**, 288–294 (2012)

29. X. Xing, X. Xiao, L. Wang, Y. Wang, Highly sensitive formaldehyde gas sensor based on hierarchically porous Ag- loaded ZnO heterojunction nanocomposites. Sensor. Actuat. B. **247**, 797–806 (2017)

30. Y.C. Feng, Y. Meng, F.X. Li, Z.P. Lv, J.W. Xue, Synthesis of mesoporous LTA zeolites with large BET areas. J. Porous Mater. **20**, 465–471 (2013)

31. T.Y. Ma, X.J. Zhang, Z.Y. Yuan, Hierarchical meso-/macroporous aluminum phosphonate hybrid materials as multifunctional adsorbents. J. Phys. Chem. C **113**, 12854–12862 (2009)

32. M. Singh, B. Yadav, A. Ranjan, M. Kaur, S. Gupta, Synthesis and characterization of perovskite barium titanate thin film and its application as LPG sensor. Sensor. Actuat. B **241**, 1170–1178 (2017)

33. L. Zhu, W. Zeng, Room-temperature gas sensing of ZnO-based gas sensor. Sensor. Actuat. A phys. **267**, 242–261 (2017)

34. B. Ostrick, J. Muhlsteff, M. Fleischer, H. Meixner, T. Doll, C. Kohl, Adsorbed water as key to room temperature gas- sensitive reactions in work function type sensors: the carbonate–carbon dioxide system. Sensor. Actuat. B **57**, 115–119 (1999)

35. C. Michel, A. Pereciado, R. Parra, C. Aldao, M. Ponce, Novel CO_2 and CO gas sensor based on nanostructured Sm_2O_3 hollow microspheres. Sensor. Actuat. B **202**, 1220–1228 (2014)